Cross sections for ionizaton of gases by 5—4000-keV protons and for electron capture by 5—150-keV protons

M. E. Rudd
University of Nebraska—Lincoln, Lincoln, Nebraska 68588-0111
and Battelle Pacific Northwest Laboratories, Richland, Washington 99352

R. D. DuBois, L. H. Toburen, and C. A. Ratcliffe
Battelle Pacific Northwest Laboratories, Richland, Washington 99352

T. V. Goffe
University of Nebraska—Lincoln, Lincoln, Nebraska 68588-0111
(Received 16 May 1983)

Using the parallel-plate-capacitor method and a capacitance manometer to determine pressures, total cross sections for the production of positive and negative charges were measured for 5—4000-keV-proton impact on He, Ne, Ar, Kr, H_2, N_2, CO, O_2, CH_4, and CO_2. From these, ionization and electron-capture cross sections were obtained and fitted to semiempirical equations describing the energy dependence in terms of a few parameters. At high energies very good agreement is obtained in the comparison of the ionization cross sections to earlier proton- and electron-impact measurements and with theoretical treatments where they are available, but discrepancies exist for some targets at low energy. Above 10 keV the electron-capture cross sections are in agreement with earlier work for all the targets except CO and CH_4 for which they are (20—40)% higher.

INTRODUCTION

The fundamental importance of the phenomenon of ionization by positive-ion impact has been recognized for a long time. Besides its theoretical interest as one of the basic collision phenomena, there are numerous applications for which ionization cross sections for specific targets are needed. A few of the areas of study which make use of such data are stellar and upper atmospheric work, radiation damage in solids, surface bombardment, thermonuclear fusion, track studies in nuclear emulsions, health physics, and plasma physics.

While considerable effort has been expended in developing theoretical treatments of the ionization process, reasonably accurate cross sections for proton ionization have been obtained only for a few targets and only for high energies. Therefore, experiment must supply most of the cross sections both for applications and to guide further theoretical work. Although an attempt was made by Goldman[1] in 1931 to detect ionization by ion impact, the first successful measurement was not made until 1949 by Keene[2] who used H^+, H_2^+, and He^+ beams on H_2 and He. A few additional measurements were made in the 1950s.[3–6] In the 1960s many additional measurements were made on a variety of targets,[7–17] but except for the recent measurements on atomic and molecular hydrogen by Shah and Gilbody,[18] there have been no systematic measurements of proton ionization cross sections reported since 1967.

Starting in the early 1960s more detailed studies of the electron ejection process were made by measuring the doubly differential cross sections for electron emission as a function of angle and energy of the electrons. While these data have been of great value in furthering our understanding of the ionization process, the total ionization cross sections obtained by integration of the doubly differential cross sections have generally not been as accurate as those of more direct measurements.

While the studies to date have yielded the general dependence of cross section on impact energy, there are sizable areas of quantitative disagreement. At the higher energies (greater than, for example, 300 keV) there are discrepancies of 20% among the few data available. In the middle range of 50—300 keV discrepancies of 50% are common, and at the lower energies reported values differ by factors as great as 3 or 4. None of the previous measurements has encompassed more than a fraction of the energy range of interest.

In the present work we have made a comprehensive set of measurements over a wide energy range (5—4000 keV) for 10 different target gases using the same experimental apparatus. This utilized the well-known parallel-plate-capacitor method pioneered by Goldman.[1] Data were taken at small energy intervals (increments of approximately 20%) in order to provide complete coverage.

The cross sections measured were gross cross sections for the production of positive and negative charge. To provide a more complete picture of the processes taking place, we have also made a series of time-of-flight measurements to determine the fractions of the various charge states produced by the collisions in various gases. Normalizing to the present ion production data will then give cross sections for production of each charge state. This

study will be reported separately.

In most proton collisions only one target electron is involved and, in this experiment, in order to produce a measurable effect this electron must either be transferred from the target to the projectile or be released to the continuum. In the latter case it contributes both to the positive-ion production cross section σ_+, and to the electron production cross section σ_-. In the former case it contributes to σ_+ only. Therefore, we can obtain the electron-capture cross section σ_c from the relation $\sigma_c=\sigma_+-\sigma_-$. With a more careful analysis, it can be shown that this relation holds even in cases where more than one electron is involved provided only that the cross section for producing H^- in the beam is negligible. While there are more accurate methods of obtaining the capture cross sections, we have included that data here since for some gases it is not available in the present literature. In cases where it has previously been measured, a comparison provides a valuable check on our results.

EXPERIMENTAL APPARATUS

Accelerators

Three different accelerators at the Battelle Pacific Northwest Laboratories and one at the University of Nebraska (UNL) were used in this experiment to cover the entire energy range with generous amounts of overlap. A tandem Van de Graaff accelerator provided energies from 1700 to 4000 keV while a single stage Van de Graaff covered the range of 100 to 2000 keV. Energies from 5 to 100 keV were obtained by using a low-energy accelerator which obtained its potential directly from a transformer-rectifier-type power supply. A directly powered accelerator at the University of Nebraska covered the range of 40 to 350 keV.

The beams from all four accelerators were momentum analyzed. The energy scales for the two high-energy accelerators were calibrated by the use of the Li(p,n) reaction at 1.8807 MeV. The current to the analyzing magnets was read to high accuracy by digital meters and used to set the accelerating potentials to the required values. The energy scale on the two low-energy accelerators was set by using a digital or differential voltmeter to read a precision voltage divider connected directly to the probe of the rf ion source. Ions in the source are created at a potential close to that of the probe which is typically 1000 V or more above that of the high-voltage terminal.

Plate assembly

Figure 1 shows the gas cell (GC) containing the target gas, the plate assembly, consisting of the ion collector plate (IP) and electron collector plate (EP), the guard plates (GP), the grid (G), the grid frames (GF), the Faraday cup (F), and its suppressor ($S1$), the entrance collimator (C), and its suppressor ($S2$). Except as noted, the entire system was made of stainless steel with machinable ceramic insulators. The collimator was made of tantalum and had an aperture of 1.5 mm (1.3 mm at Nebraska). $S2$ was kept at a negative potential to prevent secondary electrons originating at C from entering the measurement region. The bottom of the Faraday cup was made of tantalum. The gas cell and plate assemblies used at the two laboratories were made according to the same plans with only minor variations.

The grid consisted of parallel stainless-steel wires 0.038 mm in diameter spaced 1.59 mm apart running perpendicular to the beam direction. The plate assembly was symmetric except that a grid was installed only on the side adjacent to the ion collection plate to prevent the loss of secondary electrons from that plate. The secondaries from the electron collector plate were unable to leave because of the potential hill provided by the collection field and therefore no grid was needed. However, the empty grid frame was provided with the proper potential to maintain the uniform field in that region. At UNL a double-layered grid of the same wire and the same spacing was used, one layer placed 1.59 mm above the other.

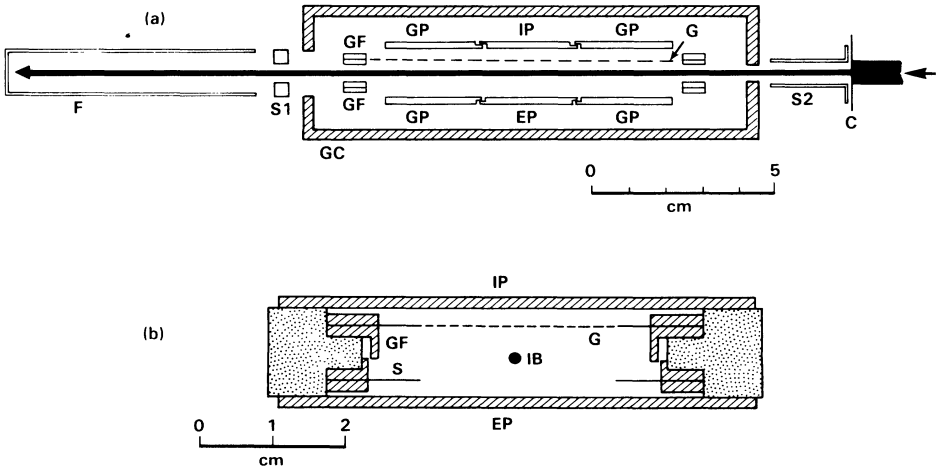

FIG. 1. (a) Side view of plate assembly. IB is the ion beam from the accelerator, C the collimator, $S2$ the suppressor, GC the gas cell, F the Faraday cup, $S1$ the cup suppressor, IP the ion plate, EP the electron plate, GP the guard plates, GF the grid frames, and G the grid. (b) End view of plate assembly. S designates the shields; other symbols as in (a).

The sides of the grid frames were made with overlapping rims so that as the beam passed between the plates it was not exposed to any insulating material. This was to prevent a possible buildup of charge on insulating surfaces which could have deformed the collection field.

Computer interface

A computer was used to control grid and plate potentials, to read currents, temperatures, and pressures and to calculate cross sections. Beam current to the Faraday cup and the ion and electron currents to the plates were read by three separate electrometers, the outputs of which were amplified and sent to voltage-controlled oscillators (VCO's) set to produce 5-kHz signals for full-scale readings on the electrometers. The electrometers along with their associated VCO's, optical couplers, and amplifiers were floating at the respective potentials of the plates. Three scalers read the counts from the oscillators over a 5-sec period. A picoampere source calibrated to within 2% and a frequency meter were used to calibrate the electrometer-VCO system independent of the meter reading on the electrometers. Thus we relied only on the linearity of the electrometer amplifiers and not on the scale readings.

Pressure measurement

McLeod gauges, used in most previous work of this type, are subjet to a serious error due to the pumping effect of the mercury backstreaming from the gauge to the cold trap. In this experiment we have used a capacitance manometer to measure the target-gas pressure. A stainless-steel tube 52 cm long and with a 1.1-cm inside diameter connected the manometer to the target-gas cell. This tube was copper in the Battelle apparatus. The reference side of the manometer was connected to the main chamber where the pressure was (1—2)% of the target-gas cell pressure or less.

EXPERIMENTAL PROCEDURE

Definition of the beam

As mentioned, the proton beam from each accelerator was momentum analyzed to obtain a pure beam of protons after the magnet. The energy of the beam was known to within about 0.5% from the calibration described above. The energy spread of the beam from the rf ion sources used is typically 100 eV, an amount which is unimportant even at the lowest energies used. The spread in energies of the tandem beam was somewhat larger in absolute value, but smaller relative to the beam energy.

Below 200 keV the neutralization of the beam in passing through the target gas became an important factor. As discussed elsewhere,[19] this causes two errors. A proton which is neutralized before entering the Faraday cup will not contribute to the measured beam current, and second, a proton neutralized before reaching the measuring plates will produce ions and electrons, but with a different cross section than for proton impact. The two effects can be accounted for by using an equation giving the ion current in terms of the cross section σ_+ for producing ions by proton impact and the cross section σ_{n+} for producing ions by neutral hydrogen atom impact. If we let l_1 be the distance from the entrance of the gas cell to the measuring region and l_2 the distance from the measuring region to the entrance of the Faraday cup, then it is easy to show that the ion and electron currents produced by the beam in the target gas are given by

$$I_i = nlI_B\sigma_+(1+nl_2\sigma_c)+n^2lI_B\sigma_{n+}l_1\sigma_c \ , \quad (1)$$

$$I_e = nlI_B\sigma_-(1+nl_2\sigma_c)+n^2lI_B\sigma_{n-}l_1\sigma_c \ , \quad (2)$$

where l is the length of the measuring electrode and σ_c is the neutralization cross section. I_B is the measured beam current and n is the target-gas density. Values of these cross sections sufficiently accurate for this correction were obtained from the empirical equations of Green and McNeal.[20] The sum of the ionization and capture cross sections from their equations were taken to be σ_{n+}. The cross section σ_{n-} is the sum of the ionization and loss cross sections for neutrals in gases.

The tables of Green and McNeal have no values for the gases CO, CO_2, and CH_4, and so for these gases, data for nitrogen were used for this correction. The equation above assumes that the densities were sufficiently low that the exponentials involved could be approximated by the first two terms of their expansion, an assumption which was generally well satisfied in our experiment. For most gases the neutralization correction was greatest at the lowest beam energy used, 5-keV, and decreased rapidly with increasing energy. For the worst case, the correction was about 40% at 5 keV, 19% at 20 keV, and 1% at 100 keV. If we estimate the uncertainty in the correction to be 40%, this yields a 16% uncertainty in the correction to σ_- at 5 keV decreasing to less than 5% at 30 keV. The correction to σ_+ was typically half as large.

Collection of the beam

Since the magnitude of the collected beam charge enters directly into the equation for the calculation of the cross section, it is essential that the Faraday cup catch all of the beam that produces the ionization to be measured. The initial alignment of the beam defining apertures and the cup was done visually and the final adjustment was accomplished by reading beam current to the cup and to the ring-shaped suppressor around the cup as the vertical and horizontal positioning was varied. With no gas in the cell and the collection field off, the current to the suppressor ring was typically 3 orders of magnitude smaller than the beam current to the Faraday cup.

The collection field caused a deflection of the beam as it passed between the plates. This deflection was negligible except at the low beam energies where it required a reduction of the collection field. Also at low energies loss of the beam from scattering in the target gas had to be considered. Calculations of this effect using the Rutherford and the screened Coulomb scattering equations indicated that this would be an appreciable problem only for the two heaviest target gases used, krypton and argon, and

then only at the lowest energies. For the worst case (krypton at 5 keV) it was calculated that 45% of the beam would be scattered so as to miss the cup. In order to reduce this error and to improve the collection of the beam in general, the current to the suppressor was added to that measured in the cup, making, in effect, a larger cup. The calculated loss of beam in this case was 12% for krypton at 0.3 mTorr pressure and 3% for argon both at 5 keV. The cross sections for these two gases were corrected for this effect at the lower energies.

At Nebraska the potential of the suppressor $S2$ next to the beam collimating aperture was made -25 V to prevent secondaries formed at the collimating aperture from entering the plate region. The Faraday cup was biased at $+45$ V and the suppressor $S1$ next to the cup at $+18$ V. This provided a field which prevented secondaries from the cup from leaving as well as suppressing secondaries from the suppressor ring itself from being projected back into the plate region. At Battelle, the potentials for $S2$, F, and $S1$ were, respectively, -300, $+135$, and $+67$ V.

Only a few percent of the protons striking the Faraday cup are expected to be reflected as fast ions or neutrals. The cup is made fairly deep to prevent a large fraction of the reflected particles from escaping back into the collision region. Ions that do escape, however, will increase the signal currents and decrease the measured beam current, both of which increase the apparent cross sections. Data on the reflections of fast ions from surfaces is too meager to allow a calculation of this effect, but this error is believed to be small if not negligible.

Density determination

The capacitance manometer used to measure target-gas pressure was compared to another recently calibrated manometer of a different type and found to agree to within 2% over the 0–3-mTorr region. The density of the target gas was determined by the equation $n=3.535\times10^{19}PT_0/T_g$ where P is the pressure of the gas in millitorr, T_g its absolute temperature, and $T_0=273.15$ K. Since the manometer head temperature T_h was kept at 322 K, a correction for thermal transpiration was necessary. The Knudsen formula, $P_h/P_g=(T_h/T_g)^{1/2}$, is presumed to be applicable when the diameter of the tubing connecting the gas cell and the manometer is much smaller than the mean free path of the gas molecules. In our apparatus the inside diameter of the tubing is 1.1 cm while the mean free path of air molecules at 1 mTorr and 25 °C is about 5 cm. Thus the condition is only marginally satisfied. Blaauw *et al.*[21] and others have brought the Knudsen equation into question, however. While it seems to apply for apertures, it overcorrects in cases in which tubing connects the gas cell and manometer. In our case the Knudsen equation yields a 4.8% correction, but we have instead chosen to make a 2% correction in agreement with the findings of Blaauw *et al.*[21]

Target-gas pressures were 1–3 mTorr for the data taken on the tandem Van de Graaff accelerator, 1–1.5 mTorr for the Van de Graaff data, and 0.3 mTorr for the data taken on the low-energy accelerator and for the data taken at UNL. Smaller beam neutralization effects at the higher energies allowed the use of larger pressures which could be read more accurately. The reduced pressures required at the lower energies had to be read on the most sensitive range of the manometer, requiring special care to minimize the drift of the pressure in the gas cell and the zero drift of the manometer. The computer continuously monitored the pressure, thus eliminating the first problem while frequent resetting of the zero control on the manometer minimized the second error. The pressure was monitored to within 1% at the pressures used at the higher beam energies and to within 3% at lower energies. We estimate the uncertainty due to zero drift of the manometer to be 1.5% at high energies and 4% at low energies. The nonzero reference pressure contributes an error of no more than 2%. Combining these with a possible 3% thermal transpiration correction error and a 2% uncertainty in the gauge calibration, we have a 6% uncertainty in density determination at the lower energies and 4% at the higher energies.

The purity of the various target gases as stated by the supplier, was at least 99.9%. Target gas was admitted to the chamber through a needle valve and a 6.4-mm-diameter pipe. The residual gas background inside the target-gas cell was typically less than 10^{-6} Torr in the UNL chamber and about 6×10^{-6} Torr at Battelle. The base pressure in the main chamber was 2×10^{-8} Torr at Battelle and 5×10^{-8} Torr at UNL. Density gradients due to the flow of target gas were small since the small aperture admitting the beam was essentially the only place from which gas escaped from the cell. The measured currents to the two collector plates were found to be linear with pressure to within a few percent over the range of pressures used in the experiment.

Collection of slow ions and electrons

Calculations using the screened Coulomb potential and also measurements in our laboratory[22] indicate that the vast majority of recoil ions from monatomic gases have very small energies, less than 1 eV. Therefore, for ions a very small collection field will suffice. Even for molecular targets the recoil energies are generally less than 10–20 eV (Ref. 22) and present no collection problems, except perhaps at the lowest beam energies. Electrons, however, have much greater energies of ejection as well as a distribution of angles relative to the beam. The collection field must be large enough to attract all but a negligible fraction of ejected electrons to the electron plate. Since the distribution of electron energies depends on the proton impact energy, the collection field needs to be varied with proton energy. An upper limit to the field is set by the deflection of the beam causing part of it to miss the cup. The lower limit is the minimum needed to prevent electrons from reaching the grid. At the lower energies an additional limitation on the minimum field results from the necessity of keeping at least a 10-V bias between the ion collection plate and the grid while still keeping the ion plate negative relative to the source (i.e., the beam path).

In addition, one must also ensure that electrons ejected

in the forward direction are collected. Because of the phenomenon of electron capture to the continuum,[23,24] there is a component of the electron distribution which has a forward velocity equal to that of the incident protons. Kim[25] has estimated that this component may involve as many as 30% of all ejected electrons in the proton energy range of 100 to 500 keV. The usual assumption in this type of measurement is that electrons formed next to the electron plate, which have velocities such as to carry them forward out of the measurement region, are compensated for by electrons formed between the previous guard plates which reach the measuring plate. This argument breaks down if an appreciable number of electrons have forward velocities which will carry them farther than the length of the guard plate. The potentials on the electrodes needed to collect the forward ejected electrons is proportional to the beam energy. With the dimensions of our apparatus it can easily be shown that the minimum potential needed is $V_g = 0.091E$, where E is the proton energy in keV. This condition was satisfied in our experiment up to about 2 MeV. At higher energies the charge transfer to the continuum process becomes much less important.

Even knowing the angular and energy distributions of ejected electrons for various proton energies,[26] it is difficult to calculate exactly the grid potential V_g needed to prevent electrons from reaching it, but by making simplifying assumptions an approximate lower limit of $V_g = 2E^{1/2}$ is obtained where E is the proton beam energy in keV. This was verified for some energies by running a saturation curve such as the one shown in Fig. 2(a). The operating point was well within the flat or saturated region. The ion-plate potential V_i was chosen to be $\frac{1}{2}V_g$ to optimize the suppression of secondary electrons from the ion collection plate; more about this in the next section. The potential of the electron collection plate V_e was always made equal to $-1.6V_g$ (except when the saturation curve was being run) to place the center of the beam in a region where the potential was zero. The value of V_g was -200 V for the later Van de Graaff and the tandem data, -60 V for the early Van de Graaff runs and for the UNL data. For the data taken on the low-energy accelerator, V_g was varied from -15 to -100 V as the beam energy was varied in order to satisfy the restrictions mentioned above.

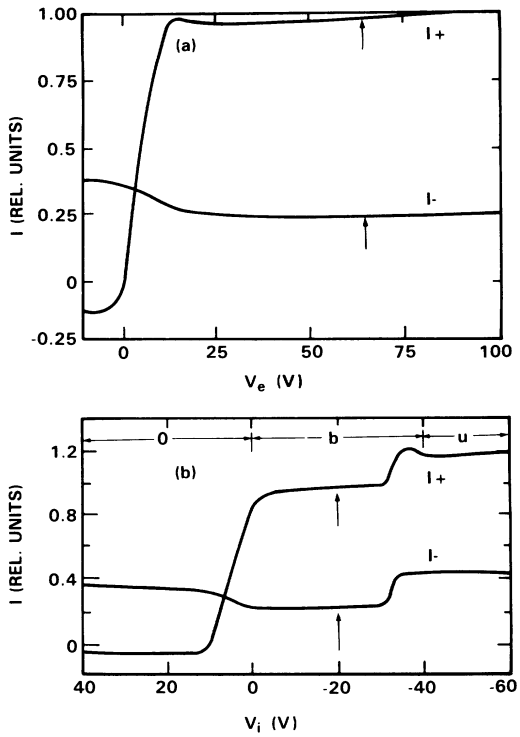

FIG. 2. (a) Saturation curve for 30 keV H^+ on helium. Ion current I_+ and electron current I_- plotted vs electron-plate potential V_e. Grid potential $V_g = -40$ V, ion-plate potential $V_i = -20$ V. Arrows indicate the operating point. (b) Bias curve for 30 keV H^+ on helium. Ion current I_+ and electron current I_- vs ion-plate potential V_i. Grid potential $V_g = -40$ V, electron-plate potential $V_e = 64$ V. Note the three regions: u is underbiased, b is biased, and o is overbiased. Arrows indicate the operating point.

Spurious processes

In a measurement of this kind, one must not only collect all of the ions and electrons from the process to be studied, but must also make sure that no spurious currents are present. The possible ways we will consider in which spurious currents are involved are (1) the production of secondary electrons at the ion plate and grid by slow ions, (2) photoelectron production, (3) secondary electrons produced at the grid by scattered beam particles, and (4) the acceleration of ions and electrons from the regions of the cup and the suppressors into the measurement region. It should be noted that all four of these effects tend to make the measured electron current greater than the ion current.

Figure 2(b) shows a typical bias curve in which the collection field between the grid and the electron plate is held fixed while the ion-plate potential V_i is varied over a wide range and the currents collected on the plates measured. There are three well-defined regions on the graph: the underbiased region u, where $V_i < V_g$; the biased region b, where $V_g < V_i < 0$; and the overbiased region o, where $V_i > 0$. In the overbiased case ions are unable to reach the ion collection plate and all end up on the grid. In the other cases only a fraction $1-t$ of the ions strikes the grid where t is the transparency of the grid. Since the grid is at a potential energy maximum for electrons, some fraction g of the secondaries emitted when ions strike the grid will go to the ion plate and the remaining fraction $1-g$ will go to the electron plate. However, g may be expected to vary with the potential distribution around the grid. If we use g_u, g_b, g_o to represent this fraction in the three regions, we can write the equations for the current I_+ collected by the ion plate and I_- to the electron plate for the three regions,

$$I_{+o} = -g_o \eta I_i \,, \tag{3}$$

$$I_{-o} = I_e + (1-g_0)\eta I_i \,, \tag{4}$$

$$I_{+b} = tI_i - (1-t)g_b \eta I_i \,, \tag{5}$$

$$I_{-b}=I_e+(1-t)(1-g_b)\eta I_i\ , \tag{6}$$

$$I_{+u}=tI_i+t\eta I_i\ , \tag{7}$$

$$I_{-u}=I_e+(1-t)\eta I_i+t\eta I_i\ , \tag{8}$$

where η is the secondary emission coefficient for ions striking the grid or ion-plate surfaces. Equations (3)–(8) give an accurate description of the major features of the measured bias curves such as those shown in Fig. 2(b). Equations (5) and (6) are used to calculate I_i and I_e, the ion and electron currents produced by the beam from which the cross sections σ_+ and σ_- are obtained using Eqs. (1) and (2). Although η and g_b need to be known, they occur only in a term multiplied by $1-t$ which is only a few percent. Therefore it is not necessary to know them to high accuracy. Since the slow ions strike the grid wires predominantly on the side away from the ion plate, the fraction g_b must be considerably less than 0.5. We have arbitrarily taken it to be 0.15.

The values of η in the literature[27] are given for only a few types of ions incident on atomically clean surfaces rather than the surfaces encountered in this experiment. Therefore we determined our own values of η by measuring ion- and electron-plate currents in the various bias regions. Combining Eqs. (3)–(6), we obtain

$$\eta=\left[\frac{(I_{+b}-I_{+o})(1-G/t)}{(I_{-o}-I_{-b})-G/t}\right]^{-1}\ , \tag{9}$$

where $G=g_o-g_b(1-t)$. Since the value of η in Eq. (9) is insensitive to variations of G, we can estimate G accurately enough for this correction to be slightly less than 0.5, say 0.4. This seems reasonable since in the overbiased case the ions (which are unable to reach the ion plate) are almost equally likely to strike the grid wires from either side.

In this way we obtain the following values of η: 0.152 for helium, 0.096 for neon, 0.044 for argon, 0.035 for methane, and 0.032 for hydrogen. The other target gases used yielded values of 0.02 or smaller and could not be accurately measured. However, the corrections to the cross sections in those cases are negligibly small anyway.

The possibility that uv photons produced by collisions in the target gas could produce photoelectrons when they strike the grid, the grid frames, and the plates was considered. An auxiliary experiment designed to measure the cross section for producing uv photons in the wavelength range which ejects photoelectrons from surfaces was performed on several of the gases used here. This work will be reported separately but the results indicate that the currents due to photoionization are less than 1% of the ion or electron currents. Therefore no correction was made.

We have already considered the scattering of protons out of the beam as it affects the measured beam current. It is also necessary to make an estimate of the fraction of scattered-beam particles which strike the grid in the measurement region and produce secondary electrons which will then go to either collecting plate. For the dimensions of our apparatus and assuming two secondary electrons per incident proton, we calculate that for the worst case, 5-keV protons on krypton, the spurious current produced would be less than 2% of the signal current. Furthermore, the scattering decreases as the square of the beam energy so this effect should be negligible for nearly all of our data. Scattering from the collimator edges is another possibility, but this cannot easily be calculated. The edges were made as sharp as possible to minimize this effect.

In the region of the Faraday cup and its suppressor the potential was positive relative to the scattering center. Therefore, any ions formed in the gas along the beam path near the cup would be propelled backward along the beam path and enter the region between the sets of plates. If the field between the plates is not great enough to sweep them aside to one of the guard plates before they reach the center measuring plates, they will contribute a spurious ion current. Likewise, the suppressor near the beam collimator is at a negative potential so in a similar fashion electrons formed by the interaction of the beam and the target gas at that point could be accelerated into the measurement region and add a spurious current to the electron current. By calculating trajectories of these particles, it was found that it was also possible for the field of the guard plates to deflect them so as to go around to the backside of the plates and again strike the center measuring plate. These spurious currents could be detected as bumps on a curve of measured ion current as a function of cup and suppressor potentials. Care had to be taken to select proper suppressor and cup potentials in relation to the plate potentials so as to eliminate this problem. In addition, a foil shield was put around the outside of the ion and electron plates and also around the leads from these plates.

Grid transmission

The grid used in the Battelle apparatus consisted of parallel stainless-steel wires 0.038 mm in diameter spaced 1.59-mm apart giving a 97.6% geometrical or optical transmission. At UNL twice as dense a grid was used giving a 95.2% optical transmission. Most investigators using grids for secondary electron suppression simply assume that the transparency of the grid for electrons or ions is the same as the optical transmission. However, because of the deflection of trajectories in the field surrounding the grid wires, the transparency is modified.

The ion current I_i from the target-beam interaction is divided into the current to the grid I_g and that reaching the plate I_+, so the actual transmission of the grid for ions is

$$t=I_+/(I_++I_g)\ . \tag{10}$$

Spangenberg[28] has studied the current division between grid and plate for electron tubes and finds that the ratio of the two currents is a function only of the ratio of the grid and plate potentials. He also shows that for a restricted range of potentials the following relation holds:

$$I_g/I_+=K(V_g/V_i)^n\ , \tag{11}$$

where K and n are constants. Combining,

$$t=[1+K(V_g/V_i)^n]^{-1}\ . \tag{12}$$

The transmission will equal the geometric transmission t_o only when the grid and plate potentials are in the same ratio as their distances from the source of ions which we take to be the center of the beam. Thus

$$t_o=(1+Kb^n)^{-1}, \tag{13}$$

where b is that ratio of distances. We can combine the last two equations to eliminate K, obtaining

$$t=[1+(t_o^{-1}-1)(V_g/bV_i)^n]^{-1}. \tag{14}$$

Using the measured value $b=0.545$ for our apparatus, we have plotted in Fig. 3 Eq. (14) as it stands, and also folded into a distribution of source potentials corresponding to the finite size of the beam. We find that if we take $n=\frac{1}{2}$ we can fit the shape of the measured curve of ion current versus V_i/V_g very satisfactorily in the region of $V_i/V_g=-0.5$ to 1.0 as shown in Fig. 3. We have therefore used Eq. (14) with $n=\frac{1}{2}$ and $V_i/V_g=+0.5$, the operating value used, to calculate t. For the Battelle apparatus $t=0.958$ while at UNL $t=0.929$.

Background signals

The background currents to the plates with the target gas off consisted of (1) leakage currents through the insulators supporting the grid and plates and the leakage in the feedthroughs and connecting cables, (2) ionization of the residual gas by the beam, (3) other spurious currents, especially beam particles scattered from the edges of the collimator and the secondary electrons they produce, and (4) residual effective current due to zero drift of the electrometers.

The leakage resistance from the ion or electron plate to ground was nominally 10^{13} to 10^{14} ohms but occasionally was lower. Above 20 keV the total background current was generally less than 3% of the signal current. However, at lower energies, it rose rapidly relative to the signal. This was partly because of a smaller signal due to a lower beam current and smaller cross sections but also because of difficulties in focusing the beam which gave rise to a greater number of scattered-beam particles. The worst case was that of helium for which the cross sections are the smallest. For this target the background current rose to as much as 60% of the I_- current at 5 keV. A similar but smaller background problem was encountered near the lower limits of the higher-energy accelerators. A correction for background was made in all cases where it exceeded 1% or 2% of the signal.

Treatment of experimental data

Five sets of cross-section data were taken as follows. An early set of data was taken on the Battelle Van de Graaff accelerator at the start of the experiment. After that data was completed, the plates and grid frames were coated with aquadag and additional shielding was installed. Using this modified apparatus data were taken on the low-energy accelerator. With the shields still in place the data on the Van de Graaff were retaken followed by runs on the tandem Van de Graaff. These four sets of data plus the set taken at UNL were all put on computer-disk file for further processing. The plate system at UNL was not coated with aquadag but did include shields along the grid frames.

The later Van de Graaff data were generally (25–35)% higher than the early Van de Graaff data while the UNL data were midway between. While these discrepancies have not been fully accounted for, we believe that the improvements in the apparatus and our additional operating experience justify a smaller weighting for the early Van de Graaff data in the averaging process although we did not feel justified in disregarding it entirely. Table I shows the weighting given to the various data sets. We also assigned a lower weighting to some of the runs near the low ends of the energy ranges since the beam definition was poorer under those conditions, the beam currents were smaller, and the background currents were relatively higher. In spite of our care in collimating the beam and providing

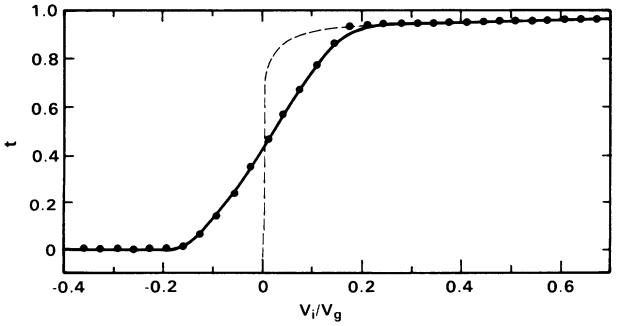

FIG. 3. Grid transmission as a function of ion-plate potential. Dashed line calculated from Eq. (14). The solid line is calculated from Eq. (14) folded into a distribution of source potentials corresponding to the beam size. Data points are actual measurements for 30 keV H^+ on helium with $V_g=-30$ V and $V_e=48$ V. Data were corrected for background and normalized at $V_i/V_g=0.25$.

TABLE I. Weighting of experimental data sets.

Data set[a]	Energy range (keV)	Weight[b]
LOW	5–30	$W=1.76E^{0.51}$
LOW	30–100	10
UNL	40–100	$W=0.1E$
UNL	100–350	10
VER	200–2000	4
VLA	100–170	$W=0.012E^{1.31}$
VLA	170–2000	10
TVD	1700–2000	5
TVD	2000–4000	7

[a]LOW is data taken on the low-energy accelerator, UNL is University of Nebraska data, VER is early Van de Graaff data, VLA is later Van de Graaff data, TVD is data taken on tandem Van de Graaff accelerator.

[b]E is beam energy in keV.

suppressors, we experienced more variability in the cross sections when an accelerator was being operated near its low-energy limit.

Data fitting

Simply averaging the data sets at each energy would result in discontinuities at the ends of the various data sets, so it was decided to make least-squares computer fits of mathematical equations to the data over the entire energy range for each target gas, adjusting the parameters for the best fit. This also has the advantage of presenting a large amount of data with a few parameters and allows the user to compute values of cross sections at energies between those actually measured without having to make interpolations.

A number of fitting equations for electron-impact ionization have been suggested,[29,30] but few have been proposed for ion impact.[20] With care, fitting equations can be found for which the parameters show some regularities from target to target and between proton- and electron-impact data for the same target. Green and McNeal[20] have made some progress along these lines.

Our values of σ_- were fitted to the equation given by Green and McNeal[20]

$$\sigma_- = (Za)^{\Omega} E^{\nu} / (J^{\Omega+\nu} + E^{\Omega+\nu}) , \tag{15}$$

where Z is the total number of electrons in the target atom or molecule a, J, Ω, and ν are adjustable fitting parameters, and E is the beam energy. The fitting was done using the CURFIT program given by Bevington.[31] Green and McNeal have taken Ω to be 0.75 while we have taken it to be a fourth fitting parameter. The average value of Ω for the ten gases was found to be 0.770 with a dispersion of only 5.9%, which confirms Green and McNeal's choice for that parameter. The dispersion of J is also reasonably small but the dispersion for a is 56%.

In order to reduce this dispersion, we have tried the approach used previously by Lotz[30] and by Rudd[32] of summing over subshells. Each electron should contribute to the cross section and all electrons in a given subshell should contribute equally. Probably the most important quantity which distinguishes one subshell from another is its binding energy I. Therefore we have expressed the proton energy E in units of the binding energy of each shell by defining the quantity $x_i = T/I_i$ where $T = E/1836$. The equation

$$\sigma_- = A\sigma_o \sum_i N_i I_i^{-2} x_i^B / (C + x_i^{D+B}) \tag{16}$$

adapted from Eq. (15) was used. Here $\sigma_o = 4\pi a_o^2 I_H^2 = 6.51 \times 10^{-18}$ m^2 eV^2, and A, B, C, and D are the fitting parameters. N_i and I_i are the number of electrons in and the binding energy of the ith subshell, respectively. Since only the outermost subshells contribute appreciably to the cross section, only those subshells indicated in Table II were included. Data for this table were obtained from Lotz,[33] Siegbahn *et al.*,[34] Hitchcock *et al.*,[35] and Rabalais and Debies.[36] The results of the fitting are given in Table III. The dispersion of A is 24%.

In the absence of a theoretical foundation we do not claim accurate predictive value for this or any other fitting equation. Nevertheless, if other information on a desired target is lacking, a potential user may wish to take advantage of these regularities and use this approach to obtain estimates of cross sections.

A fit was also made to the equation

$$\sigma_- = A\sigma_o \sum_i N_i I_i^{-2} x_i^B \ln(1 + Dx_i) / (C + x_i^{B+1}) \tag{17}$$

which again involves summing over subshell contributions. This equation has the advantage that at high energies it reduces to the $E^{-1}\log E$ form of the Bethe equation. In the low-energy limit it reduces to E^{B+1}. The parameters are given in Table IV. This equation provides a somewhat better fit to the data than the other equations, the standard deviation being less than 10% for almost all of the targets. However, the dispersions are not small, with that for D, 183%, being especially large. The unusually large value of that parameter for hydrogen distorts the average as well as the dispersion. If hydrogen is omitted, the average value of D becomes 6.54 with a dispersion of 64%.

The data were also fitted to an equation which is a generalization of an equation given by Lotz[30] for electron impact,

$$\sigma_- = A\sigma_o \sum_i N_i I_i^{-2} [1 - \exp(-Cx_i^B)] x_i^{-1} \ln(1 + Dx_i) . \tag{18}$$

TABLE II. Numbers of electrons and binding energies (in eV) for the outermost shells.

He		Ne		Ar		Kr		H_2		N_2		CO		O_2		CH_4		CO_2	
N	I	N	I	N	I	N	I	N	I	N	I	N	I	N	I	N	I	N	I
2	24.59	4	21.56	4	15.76	4	14.00	2	15.42	2	15.58	2	14.5	2	13.1	6	12.6	4	13.78
		2	21.66	2	15.94	2	14.67			4	16.9	4	17.2	2	17.0	2	22.9	4	17.32
		2	48.47	2	29.24	2	27.51			1	18.73	2	20.1	2	17.8			2	18.08
										1	25.3	2	38.3	1	18.8			2	19.36
										2	37.3			1	21.1			2	37.0
														1	25.3			2	38.6
														1	27.9				
														1	39.6				
														1	41.6				

TABLE III. Parameters for fitting Eq. (16) to σ_- data.

	A	B	C	D	Average deviation
He	1.12	1.52	2.61	0.770	8.8%
Ne	0.668	0.955	3.50	0.735	11.3
Ar	1.25	0.727	2.58	0.763	14.4
Kr	1.45	0.731	3.17	0.729	13.6
H_2	1.57	1.11	3.88	0.860	12.5
N_2	1.33	0.569	3.21	0.811	11.2
CO	1.36	0.560	3.48	0.820	13.5
O_2	0.837	0.823	2.19	0.717	12.6
CH_4	1.40	0.660	4.52	0.820	13.5
CO_2	1.03	0.710	3.11	0.770	10.2
Average	1.20	0.837	3.22	0.780	12.2
Dispersion	24%	35%	21%	6.0%	

However, this equation gives fits which are quite similar to those of the earlier equations. Since no particular advantage is seen to its use, we do not give the parameters for it. Table V gives the values of σ_- for the ten gases as calculated from Eq. (17).

The electron-capture data obtained by subtracting σ_- from σ_+ were fitted to a modification of an equation given by Green and McNeal,[20]

$$\sigma_c = A\sigma_o \sum_i N_i I_i^{-2} x_i^2 / (C + x_i^B + D x_i^F) \ . \tag{19}$$

Electron-capture cross sections determined, as in this experiment, by subtraction of two independently measured cross sections suffer in accuracy when the measured values are close together as they are at the higher energies. Only UNL data and data from the low-energy accelerator at Battelle were used in fitting the capture cross-section data since the Van de Graaff accelerator was being used near its low-energy limit in that energy range. The parameters for the fit of Eq. (19) to σ_c are given in Table VI and cross sections calculated from that fit are in Table VII.

Figure 4 shows, for three different targets, the five measured data sets along with the computer fits to Eqs. (16) and (17). The early Van de Graaff data are generally lower in value than the later set from the same accelerator and have been given a smaller weight, as mentioned previously. The tandem data generally agrees well with the later Van de Graaff data. The UNL data falls between the two sets of Van de Graaff data. In the region of overlap, the low-energy data generally fall between the UNL data and the later Van de Graaff data, but the agreement of the three is quite good for most gases.

Comparing the fits from the two equations, the curve of Eq. (17) falls slightly below that of Eq. (16) at the ex-

TABLE IV. Parameters for fitting Eq. (17) to σ_- data.

	A	B	C	D	Average deviation
He	0.413	1.16	2.18	10.6	8.7%
Ne	0.503	0.412	1.19	0.992	8.3
Ar	0.474	0.291	2.72	14.0	10.8
Kr	0.765	0.158	3.24	5.58	9.4
H_2	0.314	1.01	3.24	94.4	9.2
N_2	0.461	0.165	2.18	7.62	9.2
CO	0.443	0.241	2.30	9.05	9.9
O_2	0.517	0.180	1.66	2.68	8.7
CH_4	0.515	0.298	2.68	5.32	9.7
CO_2	0.515	0.160	1.94	3.00	7.4
Average	0.492	0.408	2.33	15.3	9.1
Dispersion	23%	90%	28%	183%	
Average[a]	0.512	0.340	2.23	6.54	9.1
Dispersion	20%	94%	27%	64%	

[a]Excluding H_2.

TABLE V. Values of σ_- given by Eq. (17). Units are 10^{-20} m^2.

Energy (keV)	He	Ne	Ar	Kr	H_2	N_2	CO	O_2	CH_4	CO_2
5	0.025	0.175	2.03	2.57	0.262	2.11	2.02	1.67	2.30	2.40
7	0.045	0.268	2.65	3.35	0.406	2.72	2.64	2.26	3.11	3.21
10	0.084	0.412	3.41	4.30	0.633	3.45	3.41	3.01	4.15	4.24
15	0.164	0.642	4.36	5.48	1.01	4.32	4.36	3.96	5.46	5.54
20	0.256	0.848	5.03	6.31	1.37	4.90	5.01	4.63	6.38	6.46
30	0.445	1.17	5.84	7.33	1.93	5.57	5.79	5.44	7.48	7.58
50	0.743	1.53	6.40	8.10	2.46	5.96	6.28	5.98	8.14	8.34
70	0.888	1.66	6.36	8.15	2.49	5.86	6.21	5.95	8.00	8.33
100	0.923	1.68	5.97	7.79	2.26	5.47	5.81	5.60	7.40	7.88
150	0.826	1.58	5.19	6.97	1.81	4.78	5.05	4.93	6.35	6.96
200	0.714	1.45	4.52	6.21	1.49	4.19	4.41	4.36	5.50	6.17
300	0.551	1.22	3.58	5.06	1.09	3.36	3.51	3.53	4.33	5.01
500	0.379	0.93	2.53	3.70	0.716	2.42	2.51	2.58	3.06	3.66
700	0.291	0.758	1.97	2.94	0.537	1.91	1.96	2.05	2.39	2.91
1000	0.219	0.600	1.49	2.26	0.395	1.46	1.49	1.58	1.81	2.25
1500	0.157	0.452	1.08	1.66	0.277	1.06	1.08	1.17	1.31	1.66
2000	0.123	0.367	0.847	1.32	0.215	0.842	0.856	0.933	1.04	1.32
3000	0.088	0.271	0.602	0.946	0.150	0.603	0.611	0.675	0.741	0.958
5000	0.057	0.182	0.388	0.617	0.095	0.392	0.396	0.445	0.481	0.630

tremes of the energy range and has a slightly flatter maximum. The fit given by Eq. (15) is nearly identical to that of Eq. (16). As always, a fitting equation is valid only over the range of the data used in the fit and users of these equations should be cautioned against using the fits outside the stated range.

The capture cross sections are plotted for two gases in Fig. 5 along with the fits from Eq. (19). The agreement between the low-energy data set and the UNL data is very good. Some difficulty was encountered in fitting the capture data since the energy range of the experiment did not extend to a sufficiently low value to encompass the maximum in the cross section for all gases. Therefore the parameter C which depends mainly on the position of the maximum could not usually be determined accurately. In fact, in one case it came out negative, indicating that the cross section would continue to rise as the energy is lowered, contrary to well verified earlier measurements. This underscores the necessity of using the fitting equations only over the range of the data used to fit them.

The σ_+ cross sections were also fitted to Eqs. (16) and (17) but since they can be obtained by adding σ_c and σ_- we have not included the parameters here. Figure 6 shows examples of σ_+ data.

Discussion of experimental uncertainties

We have already discussed the uncertainty in the measurement of density which amounts to 4% at the pressures used at the high beam energies and 6% at low energies.

TABLE VI. Parameters for fitting Eq. (19) to σ_c data.

	A	B	C	D	F	Average deviation
He	0.805	2.85	0.055	0.219	5.68	8.8%
Ne	0.162	2.78	0.007	0.026	5.53	3.8
Ar	0.380	2.51	0.000	0.065	5.87	4.4
Kr	0.485	2.51	0.009	0.081	5.60	8.8
H_2	1.044	2.88	0.016	0.136	5.86	6.4
N_2	0.374	2.73	0.002	0.109	5.32	5.8
CO	0.361	2.74	0.008	0.156	4.99	6.0
O_2	0.199	2.65	0.002	0.081	4.90	5.8
CH_4	0.474	2.20	−0.008	0.188	4.86	6.5
CO_2	0.231	2.62	0.000	0.064	5.38	8.4
Average	0.452	2.65	0.009	0.112	5.40	6.5%
Dispersion	61%	7.6%	193%	54%	7.0%	

TABLE VII. Values of σ_c given by Eq. (19). Units are 10^{-20} m^2.

Energy (keV)	He	Ne	Ar	Kr	H_2	N_2	CO	O_2	CH_4	CO_2
5	0.372	2.15	17.4	14.4	7.8	18.5	11.4	11.1	29.6	18.3
7	0.692	2.87	14.2	15.6	10.3	17.5	13.3	10.3	19.0	15.1
10	1.23	3.12	11.7	15.1	10.7	15.0	13.0	8.8	16.0	12.6
15	1.93	2.8	9.39	13.1	8.9	11.6	10.8	6.97	13.7	10.3
20	2.18	2.4	8.02	11.4	7.1	9.43	8.93	5.77	12.1	8.85
30	1.97	1.83	6.22	8.75	4.63	6.71	6.33	4.28	9.27	6.99
50	1.19	1.21	3.78	4.96	1.99	3.81	3.51	2.69	4.96	4.58
70	0.675	0.879	2.13	2.67	0.856	2.26	2.09	1.81	2.67	2.94
100	0.287	0.572	0.895	1.12	0.276	1.11	1.06	1.06	1.2	1.51
150	0.083	0.291	0.264	0.347	0.064	0.411	0.424	0.495	0.427	0.586

The uncertainty in the measurement of the beam current is due to (1) errors in the neutralization correction, (2) scattering of the beam by the target gas causing a portion of it to miss the cup, and (3) the deflection of the beam by the field between the plates. These are all negligible above 30 or 50 keV but become important at the lowest energies. Combining the worst case situations gives a 17% uncertainty at 5 keV but typically was considerably smaller than this.

Uncertainties in the plate currents can arise from (1) errors in the determination of the grid transmission, (2) errors in the correction for secondary currents, (3) photocurrents, and (4) the failure to collect all the electrons because of too low a collecting field. Our best estimate is that all these combined add only 2% uncertainty. Other spurious currents are more difficult to estimate, but may cause errors of several percent. At the lowest energies corrections for background currents may add up to 12% uncertainty at 5 keV in the worst case, but were generally much smaller.

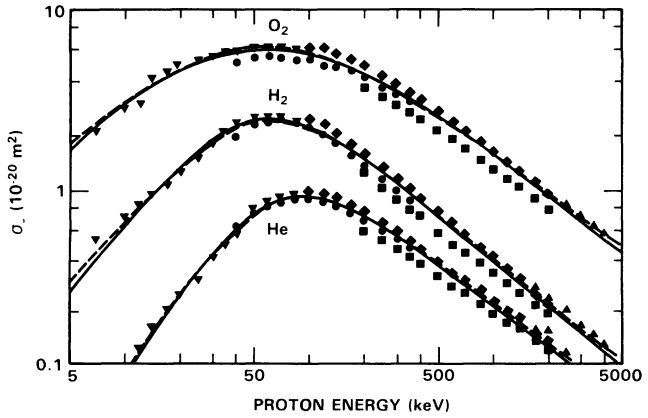

FIG. 4. Measured values of σ_- vs proton energy for He, H_2, and O_2. Low-energy accelerator, ▼; early Van de Graaff data, ■; later Van de Graaff data, ◆; tandem Van de Graaff data, ▲; UNL data, ●. Solid lines are the fits using Eq. (17), dashed lines are fits using Eq. (16).

Combining all of these, we estimate that the values of σ_- calculated from the fitting equations are uncertain by 25% at 5 keV, 20% at 10 keV, 15% at 25 keV, 10% at 100 keV, and 8% above 500 keV. These uncertainties are consistent with the average deviations of our data from the fitting curves which are from (9—12)%.

For σ_c the additional error arising from the subtraction of σ_- from σ_+ becomes important when the difference is small relative to those cross sections. Including this, the uncertainty in σ_c is 25% at 5 keV, 22% at 10 keV, 21% at 15 keV, 30% at 50 keV, and rises to 60% at 100 keV. The average deviations of the measured values from the fitting equation were only (4—9)%, well within the estimated uncertainties.

Comparison to other experimental data

Figure 7 shows a comparison between our present data, represented by the fitted curves, and earlier experimental

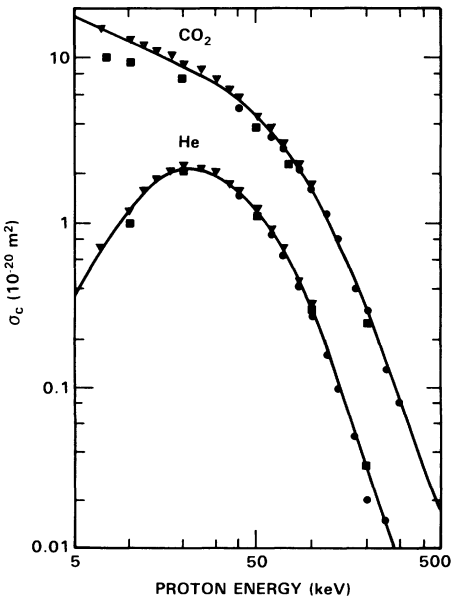

FIG. 5. σ_c vs proton energy for He and CO_2. Data from Barnett *et al.* (Ref. 38), ■. Other data points as in Fig. 4. Solid lines are the fits using Eq. (19).

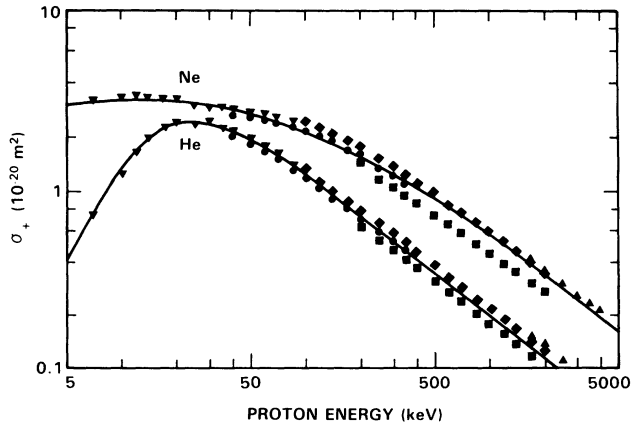

FIG. 6. σ_+ vs proton energy for He and Ne. Symbols as in Fig. 4. Solid lines are the fits using Eq. (16).

data from various investigators for three target gases. In the case of helium our results agree very closely with the data of Pivovar and Levchenko[16] at high energy and are within a few percent of Hooper's results.[8,9] They fall above the data of Gilbody and Lee[12] by about 15%. Agreement with deHeer[15] near the maximum is excellent. At the lower energies the present data agree fairly well with the results of Fedorenko *et al.*[37] but fall below most previous results. Since the cross section for helium is the smallest one measured, it is most subject to errors from contamination by other gases and from spurious electrons from a variety of sources. Also at low energies, it is difficult to ensure complete collection of the beam. All of these sources of error tend to increase the measured value of σ_- and argue for the correctness of the lowest measurement. Park and Schowengerdt[38] have measured the helium ionization cross section by integration over the energy-loss spectrum associated with ionization and they

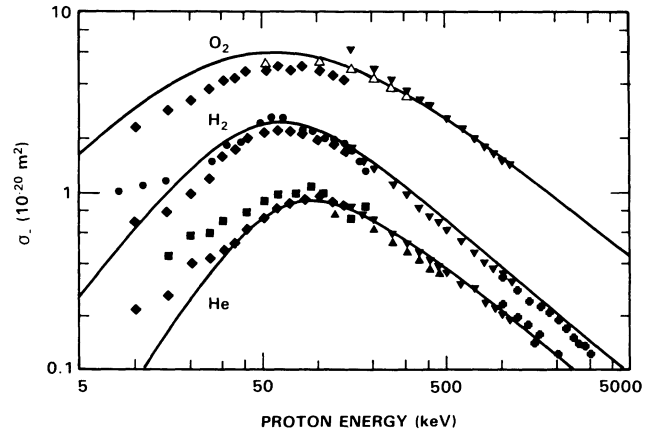

FIG. 7. Comparison of present data on σ_- as represented by the fits to Eq. (17), solid lines, and data of other investigators. Data of Solov'ev *et al.* (Ref. 11), ■; data of deHeer *et al.* (Ref. 15), ◆; data of Hooper *et al.* (Refs. 9 and 10), ▼; data of Gilbody and Lee (Ref. 12), ▲; data of Pivovar and Levchenko (Ref. 16), ✚; data of Afrosimov *et al.* (Ref. 4), ●; data of Crooks and Rudd (Ref. 39), Δ.

obtain results which are in agreement with the present results at the maximum but are lower by as much as a factor of 2 at 25 keV.

In the case of hydrogen, our data agree well with that of Hooper and of Pivovar in energy dependence at high energy but are uniformly about 18% higher. We are also about (30–35)% higher than deHeer's data in the mid range, but are in general agreement with the data of Afrosimov[4] from 15–180 keV.

Our data for oxygen agree well with Hooper's at the highest energies, but fall below it as the energy is decreased. Except for the 50-keV point, the data of Crooks and Rudd[39] are in excellent agreement with the present data. At the low energies our data are (25–30)% higher than that of deHeer. Agreement with the data of Shah and Gilbody[18] is very good.

Our high-energy data agree with that of Pivovar and Levchenko for neon, argon, and krypton to within 10% and with that of Hooper above about 200 or 300 keV. We also agree fairly well with deHeer's data from 10–20 keV but are higher than theirs by (20–25)% near the maximum for neon and argon. For krypton the agreement is within experimental uncertainty at all energies.

For nitrogen, we agree within a few percent with Hooper's data above 200 keV and with deHeer above 100 keV. However, deHeer's data falls increasingly below ours at lower energies, the discrepancy being as much as 40% from 10–25 keV. Our data for carbon monoxide agrees well with that of Hooper and although somewhat higher than the low-energy data of McNeal,[40] there is agreement within the stated limits of uncertainty. The agreement with McNeal is even better for carbon dioxide. In the case of methane, however, our cross sections are (25–35)% higher than McNeal's but still lower than those of Dessequelles *et al.*[41] Agreement with the data of Lynch *et al.*[42] for methane at 1 and 2 MeV is good.

Bethe-Born theory indicates that in the high-energy region the ionization cross sections from proton and electron impact should be equal at equal velocities. In Fig. 8 we compare our σ_- results with electron-impact data for helium, neon and nitrogen. Agreement with the data of Smith[43] and Tate and Smith[44] is well within experimental uncertainty for these gases and also for all the other gases for which data are available. The data of Schram *et al.*[45] are in generally good agreement but for some targets are lower by as much as 25%

Examples of the comparison of our electron-capture data with earlier experimental values is shown in Fig. 5 where the squares represent the recommended values given by Barnett *et al.*[46]. While our data are somewhat higher than Barnett's values, there is general agreement within the stated uncertainty except for carbon monoxide and methane where the present data are (20–40)% higher.

Comparison with theoretical calculations

In Fig. 9 we have compared our data for helium as represented by the fit to Eq. (17) with the Born-approximation calculations of Bell and Kingston[47] on a Fano plot. This graph of $E\sigma_-$ vs log$E$ has the virtue of approaching a straight line at high energy according to

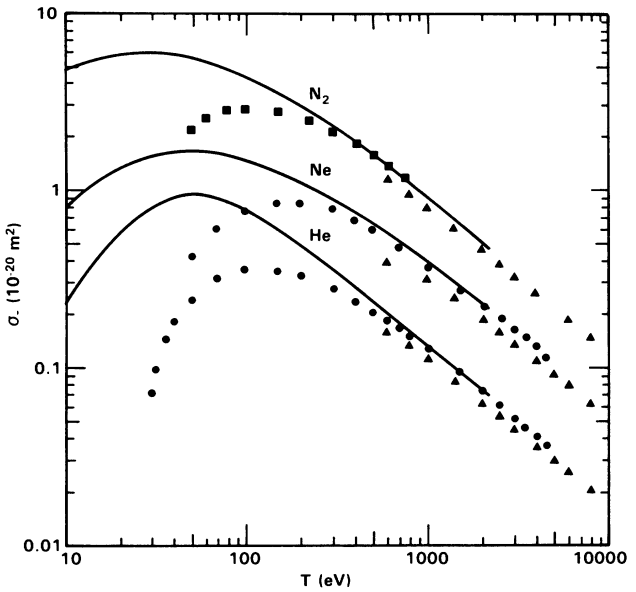

FIG. 8. Comparison of σ_- data for proton and electron impact. $T=m_e v^2/2$, where m_e is the electron mass and v is the velocity of the beam particles. Solid line is the fit of Eq. (17) to the present proton data, points are electron-impact data. Data of Smith (Ref. 43), ●; data of Tate and Smith (Ref. 44), ■; data of Schram, *et al.* (Ref. 45), ▲.

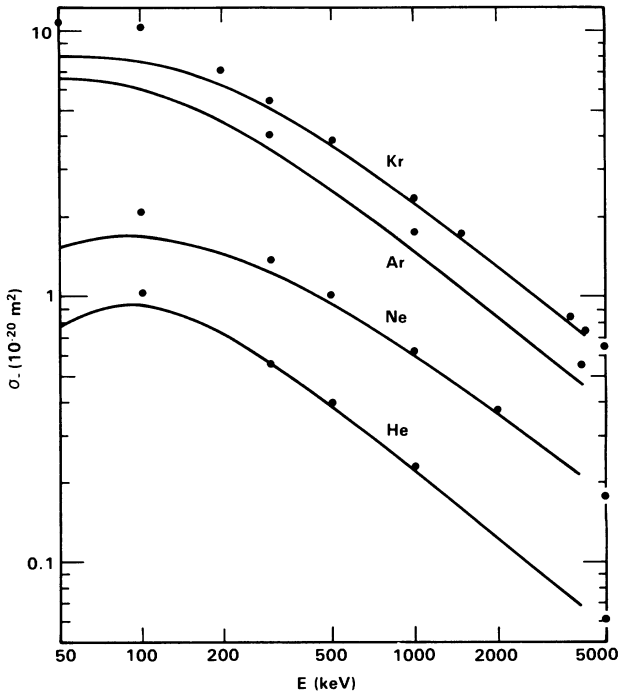

FIG. 10. Comparison of experiment and theory for proton ionization of rare gases. Solid lines are the fits of Eq. (17) to present data. Points are Born-approximation calculations (Refs. 49 and 50).

theory. Our data agree well with the calculations at the higher energies but have an area of disagreement near 50 keV. Also plotted is Eq. (15) from the paper by Inokuti and Kim.[48] In this paper they have obtained an expression for the ionization cross section for helium by subtracting measured excitation cross sections from well-known total inelastic scattering cross sections obtained from the Bethe equation. Their results should give accurate values for the magnitude and energy dependence of the cross section in the asymptotic region. This gives results in excellent agreement with the more elaborate calculations of Bell and Kingston and also in good agreement with our data.

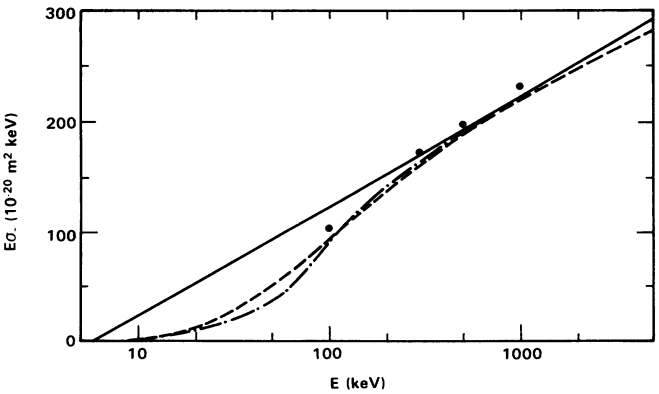

FIG. 9. Fano plot for helium. $E\sigma_-$ vs log$E$. Solid line is Eq. (15) from Inokuti and Kim (Ref. 48), dashed-dotted line is fit of Eq. (17) to present data, dashed line is the Born-approximation calculations of Bell and Kingston (Ref. 47). Dots are Born-approximation calculations using Hartree-Fock and Hartree-Slater wave functions (Refs. 49 and 50).

We have previously made calculations of differential cross sections for the rare gases using the Born approximation with Hartree-Slater and Hartree-Fock wave functions.[49,50] By integrating these, we can compare with the present experimental data as shown in Fig. 10. For krypton, the $3s$, $3p$, $3d$, $4s$, and $4p$ subshell contributions have been summed. For argon, the $2p$, $3s$, and $3p$ have been included while for neon, only the $2s$ and $2p$ contributions were used.

In the asymptotic region we note that the agreement is well within 10% except for argon where the calculated cross sections are (10—20)% above the measured values. While the agreement is gratifying for helium and neon, one would expect multiple ionization to make the measured cross sections for argon and krypton greater than the calculated values. We expect the discrepancy to be about 13% in the case of argon and 75% for krypton. Data for this estimate were obtained in an auxiliary experiment in which we used a time-of-flight method to charge analyze the slow ions produced in the collision. This work will be reported separately. We do not have an explanation for this discrepancy between theory and experiment but our excellent high-energy agreement with earlier proton and electron ionization data leads us to believe that the error lies in the calculations.

ACKNOWLEDGMENTS

The authors wish to thank Lowell Nichols for his assistance with the accelerators at Battelle and Marvin Lien

for his help in programming. We also would like to thank John Kelty who built the computer interface at UNL and did much of the programming. We would like to express our appreciation to S. T. Manson for assisting in the Born-approximation calculations. One of us (M.E.R.) would like to thank Battelle Pacific Northwest Laboratories for its hospitality while in residence during a leave of absence. This paper is based on work performed under National Science Foundation Grant No. PHY-80-25599 and the U. S. Department of Energy Contract No. DE-AC06-76RL0-1830.

[1]F. Goldman, Ann. Phys. (Leipzig) 10, 460 (1932).
[2]J. P. Keene, Philos. Mag. 40, 369 (1949).
[3]Ia. M. Fogel, L. I. Krupnik, and B. G. Safronov, Zh. Eksp. Teor. Fiz. 28, 589 (1955) [Sov. Phys.—JETP 1, 415 (1955)].
[4]V. V. Afrosimov, R. N. Il'in, and N. V. Fedorenko, Zh. Eksp. Teor. Fiz. 34, 1398 (1958) [Sov. Phys.—JETP 7, 968 (1958)].
[5]H. B. Gilbody and J. B. Hasted, Proc. R. Soc. London, Ser. A 240, 382 (1957).
[6]N. V. Fedorenko, V. V. Afrosimov, R. N. Il'in, and E. S. Solov'ev, *Proceedings of the Fourth International Conference on Ionization Phenomena in Gases, Uppsala, 1959* (North-Holland, Amsterdam, 1960), Vol. I, p. 47.
[7]Wade L. Fite, R. F. Stebbings, David G. Hummer, and R. T. Brackman, Phys. Rev. 119, 663 (1960).
[8]E. W. McDaniel, J. W. Hooper, D. W. Martin, and D. S. Harmer, *Proceedings of the Fifth International Conference on Ionization Phenomena in Gases, Munich, 1961* (North-Holland, Amsterdam, 1962), Vol. I, p. 60.
[9]J. W. Hooper, E. W. McDaniel, D. W. Martin, and D. S. Harmer, Phys. Rev. 121, 1123 (1961).
[10]J. W. Hooper, D. S. Harmer, D. W. Martin, and E. W. McDaniel, Phys. Rev. 125, 2000 (1962).
[11]E. S. Solov'ev, R. N. Il'in, V. A. Oparin, and N. V. Fedorenko, Zh. Eksp. Teor. Fiz. 42, 659 (1962) [Sov. Phys.—JETP 15, 459 (1962)].
[12]H. B. Gilbody and A. R. Lee, Proc. R. Soc. London, Ser. A 274, 365 (1963).
[13]H. B. Gilbody and J. V. Ireland, Proc. R. Soc. London, Ser. A 277, 137 (1963).
[14]Yu. S. Gordeev and M. N. Panov, Zh. Tekh. Fiz. 34, 857 (1964) [Sov. Phys.—Tech. Phys. 9, 656 (1964)].
[15]F. J. de Heer, J. Schutten, and H. Moustafa, Physica (Utrecht) 32, 1766 (1966).
[16]L. I. Pivovar and Yu. Z. Levchenko, Zh. Eksp. Teor. Fiz. 52, 42 (1967) [Sov. Phys.—JETP 25, 27 (1967)].
[17]V. V. Afrosimov, Yu. A. Mamaev, M. N. Panov, and V. Uroshevich, Zh. Tekh. Fiz. 37, 717 (1967) [Sov. Phys.—Tech. Phys. 12, 512 (1967)].
[18]M. B. Shah and H. B. Gilbody, J. Phys. B 14, 2361 (1981); 15, 3441 (1982).
[19]M. E. Rudd and J. H. Macek, Case Stud. At. Phys. 3, 47 (1972).
[20]A. E. S. Green and R. J. McNeal, J. Geophys. Res. 76, 133 (1971).
[21]H. J. Blaauw, R. W. Wagenaar, D. H. Barends, and F. J. de Heer, J. Phys. 13, 359 (1980).
[22]J. B. Crooks, Ph.D. thesis, University of Nebraska, 1974 (unpublished).
[23]Joseph Macek, Phys. Rev. 1, 235 (1970).
[24]G. B. Crooks and M. E. Rudd, Phys. Rev. Lett. 25, 1599 (1970).
[25]Yong-Ki Kim, Rad. Res. 64, 96 (1975).
[26]See, e.g., M. E. Rudd, L. H. Toburen, and N. Stolterfoht, At. Data Nucl. Data Tables 23, 405 (1979).
[27]See, e.g., Homer D. Hagstrum, Phys. Rev. 104, 672 (1956).
[28]Karl Spangenberg, *Vacuum Tubes* (McGraw-Hill, New York, 1948), p. 224.
[29]H. W. Drawin, Z. Phys. 164, 513 (1961).
[30]Wolfgang Lotz, Z. Phys. 206, 205 (1967).
[31]Philip R. Bevington, *Data Reduction and Error Analysis for the Physical Sciences* (McGraw-Hill, New York, 1969).
[32]M. E. Rudd, Phys. Rev. A 20, 787 (1979).
[33]Wolfgang Lotz, J. Opt. Soc. Am. 57, 873 (1967).
[34]K. Siegbahn, C. Nordling, G. Johansson, J. Hedman, P. F. Heden, K. Hamrin, U. Gelius, T. Bergmark, L. O. Werme, R. Manne, and Y. Baer, *ESCA Applied to Free Molecules* (North-Holland, Amsterdam, 1971).
[35]A. P. Hitchcock, C. E. Brion, and M. J. Van der Wiel, Chem. Phys. 45, 461 (1980).
[36]J. Wayne Rabalais and Tom. P. Debies, J. Electron. Spectrosc. Relat. Phenom. 5, 847 (1974).
[37]N. V. Fedorenko, V. V. Afrosimov, R. N. Il'in, and E. S. Solov'ev, *Proceedings of the Fourth International Conference on Phenomena in Ionized Gases, Uppsala, 1959* (North-Holland, Amsterdam, 1960), Vol. I, p. 47.
[38]John T. Park and F. D. Schowengerdt, Phys. Rev. 185, 152 (1969).
[39]J. B. Crooks and M. E. Rudd, Phys. Rev. A 3, 1628 (1971).
[40]R. J. McNeal, J. Chem. Phys. 53, 4308 (1970).
[41]J. Desequelles, G. D. Cao, and M. Dufay, C. R. Acad. Sci. Ser. B 262, 1329 (1976).
[42]D. J. Lynch, L. H. Toburen, and W. E. Wilson, J. Chem. Phys. 64, 2616 (1976).
[43]Philip T. Smith, Phys. Rev. 36, 1293 (1930).
[44]John T. Tate and P. T. Smith, Phys. Rev. 39, 270 (1932).
[45]B. L. Schram, F. J. de Heer, M. J. van der Wiel, and J. Kistemaker, Physica (Utrecht) 31, 94 (1964).
[46]C. F. Barnett, J. A. Ray, E. Ricci, M. I. Wilker, E. W. McDaniel, E. W. Thomas, and H. B. Gilbody, Oak Ridge National Laboratory Report No. ORNL-5206 (unpublished).
[47]K. L. Bell and A. E. Kingston, J. Phys. B 2, 653 (1969).
[48]Mitio Inokuti and Yong-Ki Kim, Phys. Rev. 186, 100 (1969).
[49]L. H. Toburen, Steven T. Manson, and Yong-Ki Kim, Phys. Rev. A 17, 148 (1978).
[50]L. H. Toburen and Steven T. Manson, *Abstracts of the Eleventh International Conference on the Physics of Electronic and Atomic Collisions, Kyoto, 1979*, edited by K. Takayanagi and N. Oda (The Society for Atomic Collisions Research, Kyoto, 1979), p. 628.